*photonics*

MDPI

*Article*

# Common-Mode Suppression of Ambient Temperature-Induced Phase Drift in Phase-Stabilized RF Fiber Links Using Dual Optical Carriers

**Wenyu Wang, Wenxuan Wang, Chuye Quan and Zhenzhen Xu ***

The School of Electronic Information Engineering/School of Integrated Circuits, Nanjing University of Industry Technology, Nanjing 210093, China
* Correspondence: 2025101570@niit.edu.cn

**Abstract**

Ambient temperature fluctuations of system environments can significantly degrade the stability of fiber-based phase-stabilized RF transfer systems. In this work, the underlying mechanism of such degradation is systematically investigated. It is shown that, in conventional single-ended architectures, temperature-dependent phase variations originating from the laser source and local RF components are directly accumulated in the phase-locked loop, resulting in pronounced instability. To address this issue, a symmetric dual-carrier architecture is proposed by introducing independent optical carriers at both the central and remote sites. This configuration transforms the system into a differential reference scheme, where temperature-induced phase perturbations exhibit common-mode characteristics and can be effectively suppressed. Meanwhile, the reduced reliance on erbium-doped fiber amplifier (EDFA) in the return path mitigates amplified spontaneous emission noise and temperature-sensitive gain fluctuations. Experimental results demonstrate that, under ambient temperature variations of approximately 7 °C, the link delay fluctuation is reduced from over 15 ps to about 1.2 ps. The corresponding frequency stability reaches a modified Allan deviation of $6.70 \times 10^{-19}$ at an averaging time of 10,000 s without strict temperature control. These results validate the effectiveness of the proposed approach for robust high-stability frequency transfer.

**Keywords:** phase-stabilized RF transfer; optical fiber transmission; temperature fluctuation suppression; dual-carrier architecture; frequency stability; microwave photonics

## 1. Introduction

Ambient temperature fluctuations pose a critical challenge to the stability of fiber-based phase-stabilized frequency (RF) transfer systems, particularly in practical deployment environments [1–3]. Such systems are widely used in large-scale time–frequency synchronization networks, radio astronomy arrays, and deep-space communication systems [4–6]. Phase-stabilized transmission techniques have been extensively developed to suppress fiber-induced phase noise, enabling ultra-stable frequency dissemination over long distances [7–9]. However, most existing studies primarily focus on compensating disturbances introduced by the fiber link itself, while the influence of environmental perturbations on the transmission system remains insufficiently addressed.

Early studies demonstrated the feasibility of phase-stabilized RF transmission over optical fiber using interferometric delay sensing and fiber-length compensation

Check for updates

Received: 31 August 2026
Revised: 21 September 2026
Accepted: 21 September 2026
Published: 27 September 2026

**Copyright:** © 2026 by the authors. Licensee MDPI, Basel, Switzerland. This article is an open access article distributed under the terms and conditions of the Creative Commons Attribution (CC BY) license.

techniques [10,11]. In practical applications, the transmission system is inevitably subject to ambient temperature fluctuations, which affect active components such as lasers, photodetectors, and RF electronics [12–14]. In conventional single-ended architectures, a single optical carrier serves as the reference source, and temperature-dependent phase variations originating from the laser and local RF chain are directly accumulated in the phase-locked loop [15–17]. As a result, system stability becomes highly sensitive to environmental temperature changes. Although temperature control and operating-point optimization have been explored, these approaches increase system complexity and fail to fundamentally eliminate temperature-induced instability [18–20].

Recent work has demonstrated dual-wavelength cancellation of group-delay-induced phase noise in opto-terahertz fiber links using a dual-channel round-trip noise-cancellation architecture [21]. In that work, the differential phase noise between two optical wavelengths is extracted through a dual-channel round-trip measurement to compensate group-delay fluctuations in opto-terahertz transmission. In contrast, the present work focuses on the common-mode suppression of ambient temperature-induced phase perturbations in a 50 km phase-stabilized RF fiber link by introducing independent optical carriers at the central and remote sites. To overcome this limitation, we propose a symmetric dual-carrier phase-stabilized transmission architecture. Unlike conventional dual-ended schemes that primarily focus on link noise compensation, this work reveals and experimentally verifies the common-mode suppression mechanism of ambient temperature-induced system-level phase perturbations. By introducing independent optical carriers at both the central and remote sites, the system is transformed from a single-ended reference configuration into a symmetric differential topology, in which temperature-induced phase fluctuations exhibit strong common-mode characteristics and are intrinsically suppressed. Furthermore, the underlying mechanism is analyzed in terms of temperature-dependent phase-noise transfer, showing that the proposed configuration converts the accumulation of temperature-induced phase errors into differential residuals. Experimental results under varying ambient temperature conditions demonstrate significantly reduced delay fluctuations and enhanced long-term stability. These findings provide new insight into temperature-noise coupling in phase-stabilized fiber links and establish a general approach for achieving intrinsically temperature-resilient frequency transfer.

## 2. System Architecture and Principle

Figure 1 illustrates the schematic diagram of the actively compensated phase-stabilized RF transmission system based on a distributed feedback (DFB) analog directly modulated laser (DML). Building upon previous work, the system architecture has been further optimized toward higher integration and compactness [22]. As shown in the inset at the upper right of Figure 1, key RF components are monolithically integrated to form the frequency modulation module (FMM) at the central site and the phase amplification module (PAM) at the remote site. By integrating the FMM, PAM, and associated optoelectronic components into a standard 1U chassis (see the inset at the upper left of Figure 1), the system footprint is significantly reduced, improving flexibility and adaptability for practical deployment.

The phase-stabilized transmission system operates by performing phase detection and active compensation of the round-trip signal at the central site, thereby suppressing phase noise induced by the fiber link and enabling the recovery of a highly stable RF signal at the remote site that is phase-locked to the reference source. In the system, a rubidium (Rb) atomic clock provides three coherent 100 MHz reference signals. One is used as the local oscillator for direct mixing measurement to evaluate system stability, while the other two serve as reference signals for DRO2 and DRO3 in the FMM to construct the error signal

generation chain. The output signals of DRO2 and DRO3 maintain a fixed frequency offset of 100 MHz relative to DRO1, enabling subsequent mixing and phase comparison.

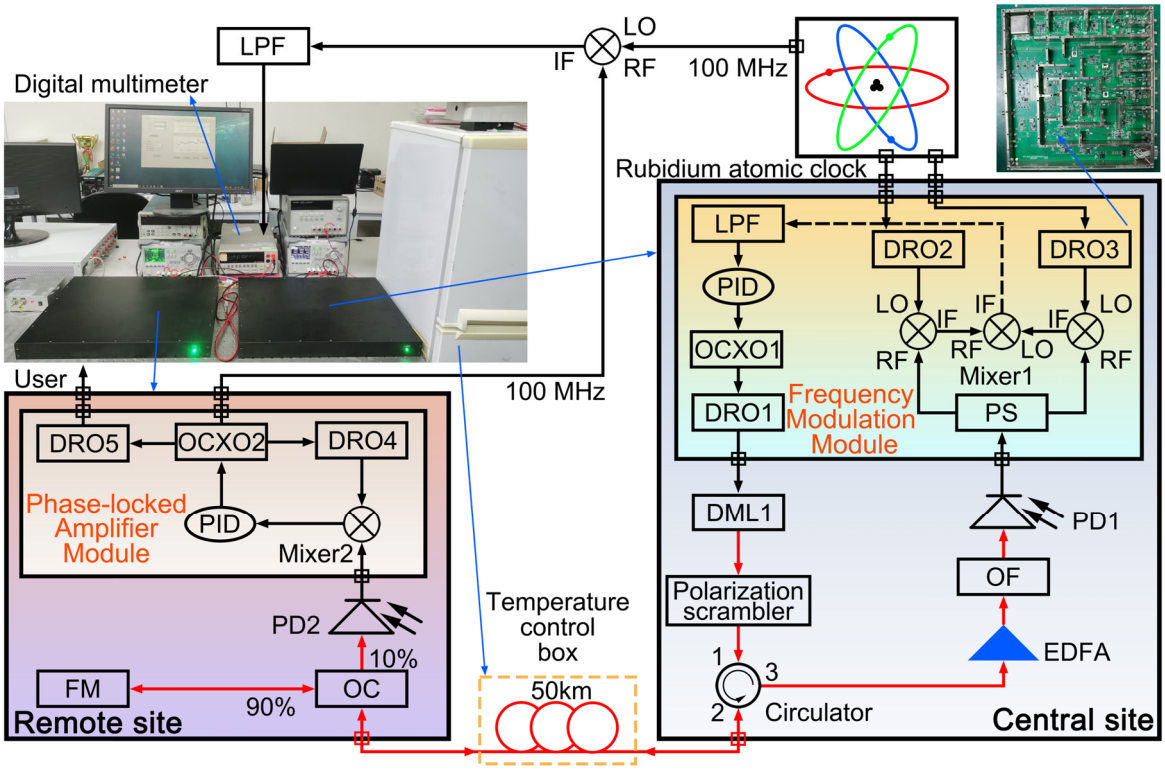



**Figure 1.** Schematic diagram of the RF signal phase-stabilized transmission system. The red lines indicate optical connections, whereas the black lines indicate RF signal connections. DRO: Dielectric resonant oscillator, OCXO: Oven-controlled crystal oscillator, PID: Proportional-Integral-Derivative, DML: Directly Modulated Laser, PS: Power Splitter, LPF: Low-Pass Filter, PD: Photodetector, OF: Optical Filter, EDFA: Erbium-Doped Fiber Amplifier, FM: Faraday Mirror, OC: Optical Coupler.

At the central site, the signal from DRO1 is used to modulate the DFB DML, generating the optical carrier. The optical signal passes through a polarization scrambler to mitigate polarization-related effects and is then launched into the 50 km fiber link via an optical circulator. At the remote site, the received optical signal is split by an optical coupler: 90% of the optical power is reflected back to the central site by a Faraday mirror, while the remaining 10% is detected by a photodetector (PD) and fed into the PAM for local signal recovery. The returned optical signal is amplified by an erbium-doped fiber amplifier (EDFA) to compensate for the fiber-link loss. Since the EDFA also introduces amplified spontaneous emission (ASE) over its gain bandwidth, the amplified signal is subsequently passed through an OF to suppress out-of-band ASE and other unwanted optical components while transmitting the desired optical carrier. OF1 and OF2 have center wavelengths of 1550.918 nm and 1550.116 nm, respectively, with a working bandwidth of less than 0.1 nm and an insertion loss of no more than 0.8 dB. The narrow passband of the OFs reduces the optical noise reaching the photodetector and thereby improves the SNR of the recovered RF signal. The resulting RF signal, containing the round-trip phase noise of the fiber link, is then fed into the FMM, where it is mixed with DRO2 and DRO3 through successive mixing stages. After low-pass filtering, the extracted error signal is fed back to the oven-controlled crystal oscillator (OCXO), enabling closed-loop control of the frequency and phase of DRO1, and ultimately achieving phase locking of the remote signal to the central reference.

To evaluate the system stability, the direct mixing method is employed to compare the phase of the recovered remote signal with that of the reference signal. By adjusting the phase difference between the two signals over a range of 0 to 2π, the phase difference can be determined from the extrema of the mixer output voltage. This allows the corresponding time delay fluctuation to be derived, from which the frequency stability of the transmission system is calculated.

## 3. Results

### *3.1. Temperature Sensitivity of the Conventional Architecture*

The temperature sensitivity of the conventional phase-stabilized transmission system shown in Figure 1 was first experimentally evaluated under laboratory ambient conditions.

As shown in Figure 2, the ambient temperature surrounding the system was continuously monitored during the experiment. The entire system was placed on an optical platform in a laboratory environment. Due to frequent human activity and day-night temperature variations, the ambient temperature exhibited noticeable fluctuations, ranging from approximately 24 °C to 29.5 °C over the measurement period. During the approximately 400,000 s test duration, the temperature variation was irregular and slowly varying.

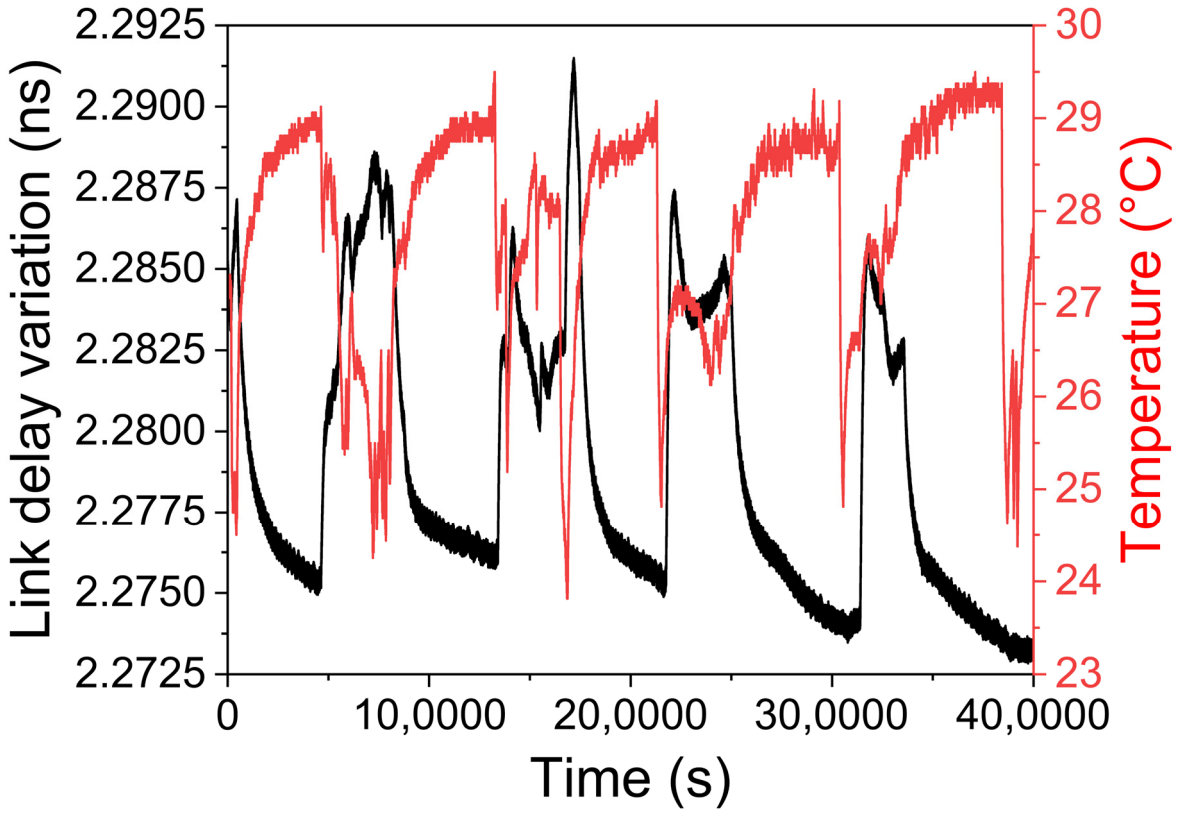



**Figure 2.** Ambient temperature variation (red line) and corresponding link delay fluctuation (black line) of the phase-stabilized transmission system measured simultaneously.

Meanwhile, the corresponding link-delay fluctuation obtained using the direct mixing method is also presented in Figure 2. The delay variation shows a clear dependence on the ambient temperature. During periods of relatively stable temperature, such as 40,000–50,000 s and 100,000–130,000 s, the delay fluctuation remained at a relatively low level of approximately 2.5 ps. In contrast, when the ambient temperature variation exceeded approximately 1 °C, the delay fluctuation increased significantly, with peak values exceeding 15 ps. The system remained locked throughout the measurement period, al-

though a pronounced increase in the residual delay fluctuation was observed under larger ambient-temperature variations.

### *3.2. Performance of the Optimized Dual-Carrier Architecture*

The optimized phase-stabilized transmission system shown in Figure 3 was subsequently evaluated experimentally under varying ambient-temperature conditions. To quantitatively evaluate the phase stability of the transmission system, a direct mixing method was employed [23]. The intermediate-frequency output voltage of the mixer was measured using a digital multimeter (DMM). By experimentally determining the maximum and minimum output voltages corresponding to a phase variation, the measured voltage was converted into the corresponding time-delay fluctuation according to

$$\Delta\tau(t) = \frac{1}{2\pi f}\cos^{-1}\left[\frac{2V(t) - (V_{max} + V_{min})}{(V_{max} - V_{min})}\right] \quad (1)$$

where the frequency of the reference signal is 9 GHz. The resulting time-delay fluctuation sequence was then imported into Stable32 for calculation of the modified Allan deviation (mADEV).

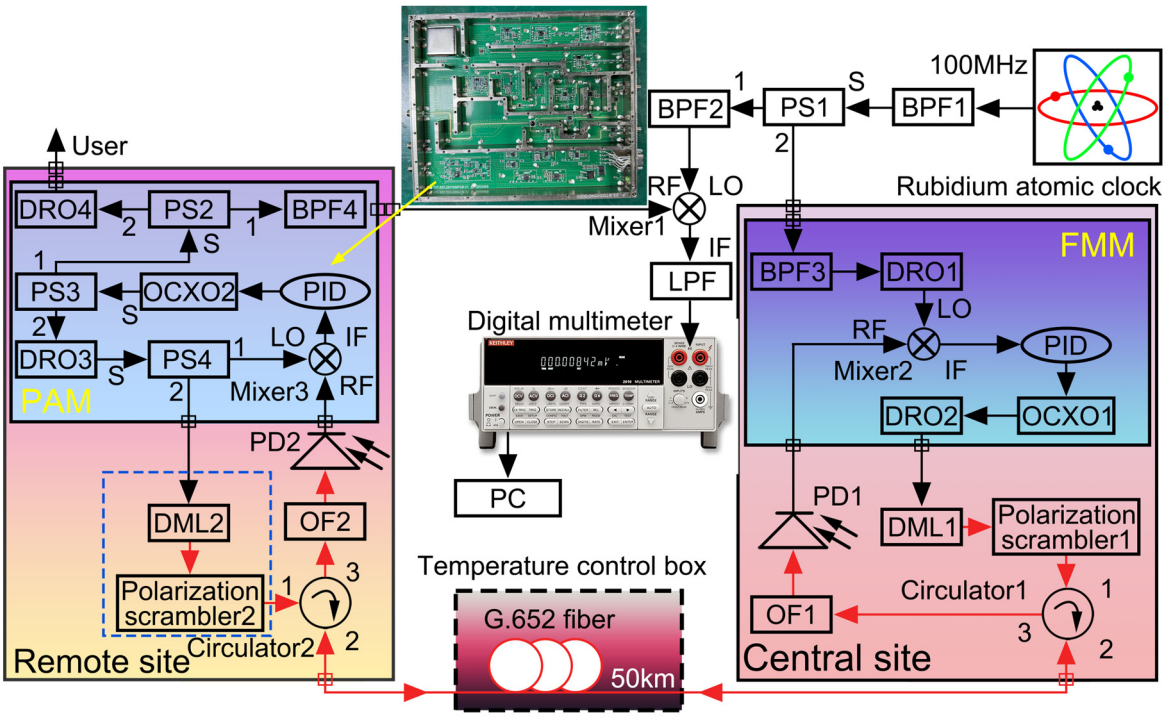



**Figure 3.** Schematic diagram of the optimized phase-stabilized transmission system based on a symmetric dual-carrier architecture for common-mode suppression of system-level temperature perturbations( The red lines indicate optical connections, whereas the black lines indicate RF signal connections).

Figure 4a shows the ambient temperature variation and the corresponding compensated link-delay fluctuation measured simultaneously. Over approximately two days, the ambient temperature fluctuated between 22.5 °C and 29.5 °C, exhibiting a clear non-stationary behavior. Under these conditions, the corresponding link-delay fluctuation is also presented in Figure 4a. The total delay variation remained within approximately 1.2 ps over the entire measurement duration.

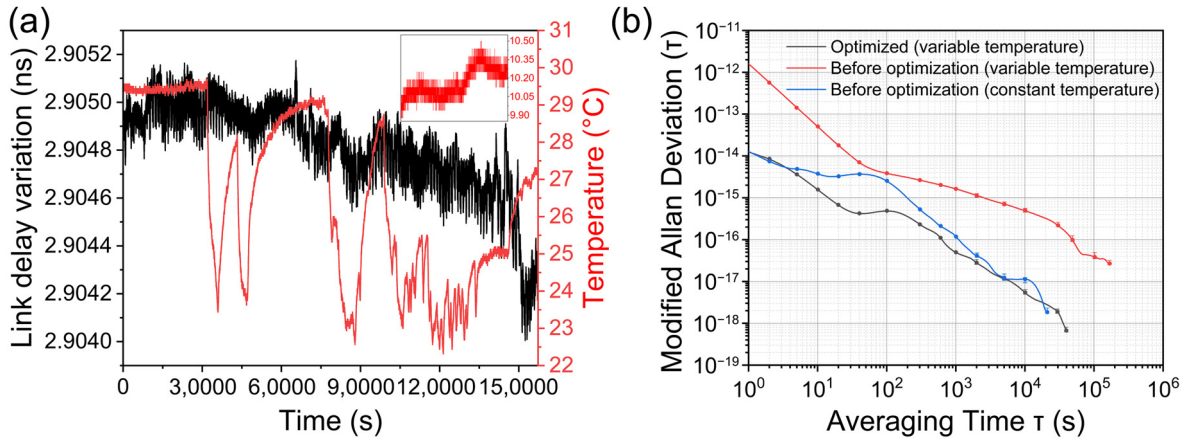



**Figure 4.** (**a**) Ambient temperature variation (red line) and corresponding compensated link delay fluctuation (black line) of the system measured simultaneously. The inset shows the temperature variation in the 50 km fiber spool inside the temperature control box, sharing the same time axis as the main panel and using the right y-axis for temperature; (**b**) comparison of system stability under different conditions (black: optimized system under varying ambient temperature; red: unoptimized system under varying ambient temperature; blue: unoptimized system under quasi-constant ambient temperature).

During the experiment, only the 50 km fiber spool was placed inside the temperature-controlled box, while the remaining optical and electronic components, including the interconnecting patch cords and OF1/OF2, were exposed to the ambient environment. The temperature variation in the 50 km fiber spool is shown in the inset of Figure 4a. Its temperature remained within 1 °C throughout the experiment, indicating a quasi-constant thermal condition.

Compared with the unoptimized system under similar ambient-temperature variations shown in Figure 2, the compensated link-delay fluctuation was reduced from peak values exceeding 15 ps to approximately 1.2 ps.

Figure 4b compares the system stability under different conditions. For the unoptimized system under varying ambient temperature (red curve), the short-term stability was $1.60 \times 10^{-12}$/s, and the stability saturated at approximately $2.71 \times 10^{-17}$/100,000 s. When the ambient temperature was stabilized (blue curve), the short-term stability improved to $1.28 \times 10^{-14}$/s, while the long-term stability reached $1.90 \times 10^{-18}$/10,000 s.

In contrast, the optimized system maintained stable performance under the same varying ambient-temperature conditions (black curve). The short-term stability remained at a similar level, while the long-term stability was improved to $6.70 \times 10^{-19}$/10,000 s.

To further evaluate the detection signal quality, the optical and RF power levels were compared between the conventional and proposed architectures. In the conventional single-carrier configuration, the DML output optical power was approximately 9.11 dBm. The optical power received by PD2 was approximately −3.1 dBm, while the returned optical power at PD1 decreased to approximately −12.44 dBm after passing through the circulator and coupler. The corresponding demodulated RF powers at PD1 and PD2 were −11.11 dBm and −23.36 dBm, respectively, with a measured RF SNR of approximately 46 dB at PD1.

In the proposed dual-carrier configuration, the optical powers received by PD1 and PD2 were approximately −3.1 dBm and −3.4 dBm, respectively, while the corresponding demodulated RF powers were −11.11 dBm and −11.21 dBm. The measured RF SNR at PD1 increased to 53.92 dB.

## 4. Discussion

### *4.1. Mechanism of Common-Mode Suppression and Phase Stabilization*

The experimental results in Section 3.1 demonstrate that the conventional single-ended architecture exhibits pronounced sensitivity to ambient temperature variations. This behavior originates from the temperature dependence of both the optical propagation path and the optoelectronic components involved in the phase-stabilization loop. In particular, temperature variations modify the fiber propagation delay through changes in both the fiber length and refractive index, while temperature-dependent characteristics of the laser and electronic components can introduce additional phase perturbations.

Taking the laser as an example, its central wavelength varies with temperature according to the established temperature dependence of semiconductor lasers [10]:

$$\Delta\lambda = k_T \Delta T \tag{2}$$

where $\Delta\lambda$ denotes the wavelength shift, $k_{\mathrm{T}}$ is the temperature coefficient of the laser wavelength, and $\Delta T$ represents the ambient temperature variation. Based on the standard expression for the optical propagation phase [24], the phase accumulated over an optical path can be written as:

$$\phi = \frac{2\pi n L}{\lambda} \tag{3}$$

where $n$ is the refractive index, $L$ is the effective propagation length, and $\lambda$ is the optical wavelength. Considering the temperature-induced wavelength variation given by Equation (2), the corresponding phase perturbation due to wavelength drift can be obtained from Equation (3) as:

$$\Delta\phi = -\frac{2\pi n L}{\lambda^2} k_T \Delta T \tag{4}$$

It can thus be concluded that temperature variations introduce phase perturbations through wavelength drift and changes in the properties of the optical and electronic components. It should be noted that, in addition to the laser, other components in the RF chain-such as mixers, amplifiers, and PDs are also affected by temperature fluctuations. Their phase response and gain characteristics may drift accordingly. Therefore, ambient temperature variations correspond to multiple coupled sources of phase error within the system.

In the single-ended reference architecture, these temperature-dependent errors are accumulated along the same reference path. The resulting output phase can be expressed as:

$$\phi_{error} = \Delta\phi_{Opt} + \Delta\phi_{Ele} \tag{5}$$

where $\Delta\Phi_{Opt}$ and $\Delta\Phi_{Ele}$ represent the equivalent temperature-induced drift terms in the optical and electrical paths, respectively. Since the system relies on a single reference source, these temperature-dependent errors cannot be suppressed through structural symmetry. Instead, they are directly transferred to the phase-locked loop (PLL) output, making the overall system stability highly sensitive to ambient temperature fluctuations.

In contrast, the proposed dual-carrier architecture transforms the temperature-induced phase perturbation from a single-ended accumulation process into a differential process. As illustrated in Figure 3, independent optical carriers are employed at the central and remote sites, allowing the phase perturbations associated with the two transmission directions to be jointly evaluated through the phase-detection process.

To address this limitation, in the optimized system shown in Figure 3, independent optical carrier reference sources are introduced at both the central site and the remote site, with wavelengths $\lambda_1$ and $\lambda_2$, respectively, where $\lambda_1 \neq \lambda_2$. Based on the above fundamental

relationships, the temperature-dependent phases of the two independent optical carriers in the proposed dual-carrier architecture can be expressed as:

$$\phi_1 = \frac{2\pi nL}{\lambda_1} \tag{6}$$

$$\phi_2 = \frac{2\pi nL}{\lambda_2} \tag{7}$$

When ambient temperature variations occur, the phases at the central site and the remote site evolve to $\Delta\Phi_1$ and $\Delta\Phi_2$, respectively. The detected differential phase is therefore obtained as:

$$\phi_{diff} = (\phi_1 + \Delta\phi_1) - (\phi_2 + \Delta\phi_2) = (\phi_1 - \phi_2) + (\Delta\phi_1 - \Delta\phi_2) \tag{8}$$

For the experimental configuration, where the central and remote units are located in close spatial proximity, their ambient temperature variations can be reasonably assumed to be strongly correlated:

$$\Delta\phi_1 \approx \Delta\phi_2 \tag{9}$$

The common-mode suppression described by Equation (9) relies on sufficient correlation between the temperature-induced phase perturbations experienced by the two transmission paths. When the environmental perturbations at the two terminals are highly correlated, the common-mode component can be effectively rejected through differential detection. In contrast, spatially or temporally uncorrelated temperature variations will produce a residual differential phase component that cannot be completely canceled.

Based on the proposed architecture and the above phase relationships, the reference signal generated at the central site can be written as:

$$S_0 = cos(\omega_0 t + \varphi_0) \tag{10}$$

where $\omega_0$ and $\varphi_0$ denote the angular frequency and phase of the reference signal, respectively. For simplicity, the amplitude of the cosine function is normalized. After compensation by the OCXO, the signal propagating from the central site to the remote site is expressed as:

$$S_1 = cos(\omega_0 t + \varphi_0 + \varphi_{com} + \Delta\varphi) \tag{11}$$

where $\Delta\varphi$ represents the propagation delay of the fiber link from the central site to the remote site, and $\varphi_{com}$ denotes the phase shift introduced by the OCXO. After being modulated and reflected back at the remote site, the round-trip signal is derived as:

$$S_2 = cos(\omega_0 t + \varphi_0 + 2\varphi_{com} + 2\Delta\varphi) \tag{12}$$

By mixing the round-trip signal with the local reference signal and feeding the resulting error signal back to the OCXO, the compensated output signal at the remote site can be derived as:

$$\begin{aligned} S_3 &= cos(\omega_0 t + \varphi_0 + \varphi'_{com} + \Delta\varphi) \\ &= cos(\omega_0 t + \varphi_0 + \varphi_{com}) \end{aligned} \tag{13}$$

Thus, phase noise induced by temperature variations and mechanical perturbations along the link is effectively suppressed.

### *4.2. Residual Differential Effects Due to Chromatic Dispersion*

Although the dual-carrier architecture can suppress the correlated component of temperature-induced phase perturbations, the two optical carriers do not experience ex-

actly identical propagation conditions because they operate at different wavelengths. In particular, chromatic dispersion introduces a wavelength-dependent group delay, resulting in a residual differential delay between the two optical carriers.

It should be noted that Equations (6) and (7) use the same refractive index $n$ as a simplified representation of the common fiber propagation path. In practice, the two optical carriers at 1550 nm and 1550.8 nm experience slightly different group delays because of chromatic dispersion. The resulting static differential delay, however, does not directly represent a temperature-induced phase error. Instead, the relevant residual error for the proposed common-mode suppression scheme is the temperature-dependent variation in the differential delay between the two wavelengths.

To evaluate this effect quantitatively, the temperature dependence of chromatic dispersion was considered. For a commercial G.652 fiber at approximately 1550 nm, the chromatic dispersion $D$ is approximately 17 ps/(nm·km), while the thermal coefficient of chromatic dispersion is approximately $\kappa = -1.45 \times 10^{-3}$ ps/(km·nm·°C), with a thermal expansion coefficient of $5.6 \times 10^{-7}$ °C$^{-1}$ [24]. The temperature sensitivity of the differential propagation delay between two wavelengths can be approximated as [25]

$$\frac{\partial \Delta \tau_{diff}}{\partial T} = \Delta \lambda L(\kappa + D\alpha) \tag{14}$$

where $\Delta\lambda = \mid \lambda_1 - \lambda_2 \mid$, $L$ is the fiber length, $\alpha$ is the thermal expansion coefficient, and $\kappa$ is the thermal coefficient of chromatic dispersion. For $\lambda_1 = 1550$ nm, $\lambda_2 = 1550.8$ nm, and $L = 50$ km, the estimated differential-delay temperature coefficient is approximately $-0.058$ ps/°C. Therefore, even if the entire 50-km fiber link were subjected to a 7 °C temperature variation, the corresponding differential delay variation would be approximately 0.40 ps. In the actual experiment, the 50-km fiber spool was maintained inside a temperature-controlled box, with its temperature variation limited to less than 1 °C, corresponding to a differential delay variation of less than approximately 0.058 ps. This value is much smaller than the approximately 1.2 ps residual link-delay fluctuation measured for the complete transmission link. Therefore, the wavelength-dependent dispersion and thermal-expansion effects are not expected to dominate the measured residual delay fluctuation under the experimental conditions.

### *4.3. Optical Crosstalk and Rayleigh Backscattering*

Bidirectional transmission over a single fiber can introduce optical crosstalk through Rayleigh backscattering and parasitic reflections at optical interfaces. These unwanted counter-propagating optical components may interfere with the desired optical signals and consequently affect the beat-note quality and phase-detection accuracy.

The influence of Rayleigh backscattering has also been investigated in previous 50-km fiber-optic RF transmission work [26]. In that system, a Faraday mirror was used at the remote site to rotate the polarization of the returned optical signal by 90°, thereby making it orthogonal in polarization to the corresponding Rayleigh-backscattered component. Experimental comparison showed that replacing the remote circulator with a Faraday mirror reduced the RF noise floor by approximately 3 dB and increased the signal-to-noise ratio from 66.61 dB to 69.65 dB [26]. These results provide experimental evidence that polarization rotation by a Faraday mirror can mitigate the influence of Rayleigh backscattering on the detected RF signal.

In the present dual-carrier system, however, a separate quantitative measurement of the optical spectrum immediately before PD1 or the change in PD1 optical power with DML1 and DML2 operated individually was not performed. Therefore, the specific

contribution of Rayleigh-backscattered DML1 light to the phase-detection signal at PD1 cannot be quantitatively isolated from the present measurements.

Nevertheless, the experimentally demonstrated phase-stabilization performance of the complete system indicates that the residual optical crosstalk under the investigated conditions did not prevent effective phase detection and phase stabilization. The use of two optical carriers together with high-isolation circulators provides an additional means of reducing the potential interaction between the counter-propagating optical signals.

A quantitative investigation of the residual optical crosstalk as a function of the wavelength separation between the two optical carriers would be valuable in future work. Such measurements could include the optical spectrum and received optical power at the photodetection points under individually controlled operation of the two lasers, providing a more direct evaluation of the contribution of Rayleigh backscattering and parasitic reflections to the phase-detection process.

### *4.4. Temperature Robustness, Limitations, and Practical Implications*

The experimental improvement observed in Section 3 can be understood from the different responses of the two architectures to environmental perturbations. In the conventional single-ended architecture, temperature-induced phase perturbations accumulate along the transmission path and are directly reflected in the residual phase fluctuation. In the proposed dual-carrier architecture, the correlated component of these perturbations is converted into a common-mode contribution and partially rejected through differential phase detection. This mechanism accounts for the substantially reduced delay fluctuation and improved long-term stability observed under varying ambient-temperature conditions.

The temperature robustness of the proposed architecture is nevertheless subject to the spatial and temporal correlation of the environmental perturbations experienced by the two transmission paths. If the temperature variations at the central and remote sites become strongly asymmetric or rapidly decorrelated, the resulting differential phase perturbation will not be fully suppressed. In addition, chromatic dispersion and residual optical crosstalk introduce differential contributions that remain outside the ideal common-mode cancellation mechanism.

To further evaluate whether the reduced dependence on EDFA amplification affects the detection signal quality, the optical and RF power levels were compared between the conventional and proposed architectures. In the conventional single-carrier configuration, the DML output optical power is approximately 9.11 dBm. The optical power received by PD2 is approximately $-3.1$ dBm, while the returned optical power at PD1 decreases to approximately $-12.44$ dBm after passing through the circulator and coupler. Therefore, EDFA amplification is required to increase the optical power at the local detection path to approximately $-3$ to $-4$ dBm. The corresponding demodulated RF powers at PD1 and PD2 are $-11.11$ dBm and $-23.36$ dBm, respectively, with a measured RF SNR of approximately 46 dB at PD1. In contrast, in the proposed dual-carrier configuration, the optical powers received by PD1 and PD2 are approximately $-3.1$ dBm and $-3.4$ dBm, respectively, and the corresponding demodulated RF powers are $-11.11$ dBm and $-11.21$ dBm. The measured RF SNR at PD1 increases to 53.92 dB. These results indicate that the reduced dependence on EDFA amplification does not compromise the effective RF detection SNR. Although a reduction in optical power could in principle increase the relative contribution of shot noise and detector noise, the received optical powers in the proposed configuration remain at approximately $-3.1$ dBm and $-3.4$ dBm, and no degradation of the measured RF SNR is observed. Furthermore, the proposed system achieves a short-term stability of approximately $1.20 \times 10^{-14}$ at $\tau = 1$ s under varying ambient temperature conditions,

demonstrating that the reduced dependence on EDFA amplification does not result in a noticeable degradation of short-term stability.

From a practical perspective, the proposed architecture provides a means of improving the temperature robustness of phase-stabilized RF fiber links without relying solely on stringent thermal stabilization of every component in the transmission system. The approach is particularly attractive for high-stability RF frequency dissemination in environments where slow or moderately varying temperature perturbations are spatially correlated. Further optimization of the optical wavelength separation, optical isolation, and environmental configuration may provide additional improvements in long-term stability.

## 5. Conclusions

The impact of ambient temperature fluctuations on fiber-based phase-stabilized RF transmission systems has been systematically investigated. In conventional single-ended architectures, temperature-dependent phase variations originating from the laser source and local RF components are directly accumulated in the phase-locked loop, leading to significant degradation of system stability. To overcome this limitation, a symmetric dual-carrier architecture is proposed, in which independent optical carriers are introduced at both the central and remote sites. By transforming the system from a single-ended reference scheme into a differential configuration, temperature-induced phase perturbations are converted into common-mode components and effectively suppressed. Experimental results show that, under ambient temperature variations of approximately 7 °C, the link delay fluctuation is reduced from over 15 ps to about 1.2 ps. Meanwhile, the frequency stability reaches a modified Allan deviation of $6.70 \times 10^{-19}$ at an averaging time of 10,000 s, even without stringent environmental temperature control. In addition, the reduced reliance on EDFA amplification reduces the contribution of EDFA-related ASE noise and temperature-dependent gain fluctuations while maintaining high-quality RF detection.

These results demonstrate that the proposed architecture significantly enhances the robustness of phase-stabilized RF transmission systems against environmental perturbations. This approach relaxes the requirement for strict thermal control and provides a practical solution for high-stability RF frequency transfer in complex and variable operating environments.

**Author Contributions:** W.W. (Wenyu Wang): Conceptualization, methodology, formal analysis, investigation, data analysis, and writing—original draft preparation. W.W. (Wenxuan Wang): Investigation, methodology, and validation. C.Q.: Investigation and formal analysis. Z.X.: Supervision, conceptualization, funding acquisition. All authors have read and agreed to the published version of the manuscript.

**Funding:** This work was supported in part by the National Natural Science Foundation of China (62404098) and the Natural Science Research of Jiangsu Higher Education Institutions of China (BK20241196).

**Institutional Review Board Statement:** Not applicable.

**Informed Consent Statement:** Not applicable.

**Data Availability Statement:** Data are contained within the article, as shown in the figures and associated descriptions.

**Conflicts of Interest:** The authors declare no conflicts of interest.

## References

1. Daddario, L.R.; Trinh, J.T. Stabilization of phase of a sinusoidal signal transmitted over optical fiber. *NASA Tech Briefs* **2010**, *34*, 31–32.

2. Zhu, X.; Wang, B.; Guo, Y.; Yuan, Y.; Gamatham, R.; Wallace, B.; Grainge, K.; Wang, L. Robust fiber-based frequency synchronization system immune to strong temperature fluctuation. *Chin. Opt. Lett.* **2018**, *16*, 010605. [CrossRef]
3. Neelam; Bharath, V.; Das, M.; Agarwal, A.; Panja, S. Transferring time and frequency signal through phase compensated telecommunication fibres. *Measurement* **2024**, *234*, 114902. [CrossRef]
4. Chen, Y.; Wang, B.; Wang, L.; Grainge, K.; Oberland, R.; Whitaker, R.; Wilkinson, A. Integrated dissemination system of frequency, time and data for radio astronomy. *IEEE Photonics J.* **2021**, *13*, 1–7. [CrossRef]
5. He, Y.; Baldwin, K.G.H.; Orr, B.J.; Warrington, R.B.; Wouters, M.J.; Luiten, A.N.; Mirtschin, P.; Tzioumis, T.; Phillips, C.; Stevens, J.; et al. Long-distance telecom-fiber transfer of a radio-frequency reference for radio astronomy. *Optica* **2018**, *5*, 138–146. [CrossRef]
6. Giorgetta, F.R.; Swann, W.C.; Sinclair, L.C.; Baumann, E.; Coddington, I.; Newbury, N.R. Optical two-way time and frequency transfer over free space. *Nat. Photon.* **2013**, *7*, 434–438. [CrossRef]
7. Newbury, N.R.; Williams, P.A.; Swann, W.C. Long distance optical frequency transfer over fiber: Predicting the frequency stability from the fiber noise. In Proceedings of the 2008 IEEE International Frequency Control Symposium, Honolulu, HI, USA, 19–21 May 2008; pp. 725–728.
8. Zhang, X.; Hu, L.; Deng, X.; Zang, Q.; Jiao, D.; Gao, J.; Wang, D.; Zhou, Q.; Liu, J.; Xu, G.; et al. Passively stable dissemination of ultrastable optical frequency via a noisy field fiber network. *Opt. Laser Technol.* **2023**, *157*, 108738. [CrossRef]
9. Zhang, A.; Dai, Y.; Yin, F.; Ren, T.; Xu, K.; Li, J.; Tang, G. Phase stabilized downlink transmission for wideband radio frequency signal via optical fiber link. *Opt. Express* **2014**, *22*, 21560–21566. [CrossRef] [PubMed]
10. Wilcox, R.; Byrd, J.M.; Doolittle, L.; Huang, G.; Staples, J.W. Stable transmission of radio frequency signals on fiber links using interferometric delay sensing. *Opt. Lett.* **2009**, *34*, 3050–3052. [CrossRef] [PubMed]
11. Tratnik, J.; Pavlovic, L.; Batagelj, B.; Lemut, P.; Ritosa, P.; Ferianis, M.; Vidmar, M. Fiber length compensated transmission of 2998.01 MHz RF signal with femtosecond precision. *Microw. Opt. Technol. Lett.* **2011**, *53*, 1553–1555. [CrossRef]
12. Akiba, S.; Utaka, K.; Sakai, K.; Matsushima, Y. Temperature dependence of lasing characteristics of InGaAsP/InP distributed feedback lasers in 1.5 μm range. *Jpn. J. Appl. Phys.* **1982**, *21*, 1736–1740. [CrossRef]
13. Amiri, I.S.; Houssien, F.M.A.M.; Rashed, A.N.Z.; Mohammed, A.E.N.A. Temperature effects on characteristics and performance of near-infrared wide bandwidth for different avalanche photodiodes structures. *Results Phys.* **2019**, *14*, 102399. [CrossRef]
14. Boudot, R.; Rubiola, E. Phase noise in RF and microwave amplifiers. *IEEE Trans. Ultrason. Ferroelectr. Freq. Control* **2012**, *59*, 2613–2624. [CrossRef] [PubMed]
15. Peng, H.; Liu, N.; Xie, X.; Chen, Z. Photonic microwave synthesizer based on optically referenced sub-sampling phase-locked optoelectronic oscillator. *Opt. Commun.* **2021**, *499*, 127304. [CrossRef]
16. Nash, G. *Phase-Locked Loop Design Fundamentals*; Motorola Application Note AN535; Motorola: Schaumburg, IL, USA, 1994.
17. Hasan, M.; Nicholls, C.; Hall, T. On the stability & phase locking to a system reference of an optoelectronic oscillator with large delay. *Sci. Rep.* **2023**, *13*, 4207. [CrossRef] [PubMed]
18. Bercy, A.; Lopez, O.; Pottie, P.E.; Amy-Klein, A. Ultrastable optical frequency dissemination on a multi-access fibre network. *Appl. Phys. B* **2016**, *122*, 189. [CrossRef]
19. Yang, J.; Zou, C.; Lin, C.; Zhu, Y.; Zhu, Y.; Dang, F.; Yuan, Y.; Yu, Z.; Wang, Y.; Qin, Y. Noise compensation methods for optical fiber frequency sweeping interferometry: A review. *J. Light. Technol.* **2023**, *41*, 4035–4050. [CrossRef]
20. Wang, L.X.; Zhu, N.H.; Liu, J.G.; Li, W.; Zhu, H.; Wang, W. Experimental optimization of phase noise performance of optoelectronic oscillator based on directly modulated laser. *Chin. Sci. Bull.* **2012**, *57*, 4087–4090. [CrossRef]
21. Heffernan, B.M.; Greenberg, J.; Mcgrew, W.F.; Rolland, A. Dual-wavelength cancellation of group-delay-induced phase noise in opto-terahertz fiber links. *J. Opt. Soc. Am. B* **2026**, *43*, 1702–1709. [CrossRef]
22. Yin, Z.Q.; Zhou, X.; Peng, P.; Guan, S.J.; Gang, Z.Y.; Zhang, C.B.; Nie, J.Q.; Li, Z.Z.; Wang, Z.Y.; Tang, K.F.; et al. Analysis of the impact of DFB analog direct modulation laser and optical link configuration on the performance of a 50 km spool fiber phase-stabilized transmission system. *Opt. Laser Technol.* **2025**, *184*, 112565. [CrossRef]
23. Yin, Z.Q.; Zhang, C.; Guan, S.J.; Zhou, X.; Wang, Y.G.; Wang, L.L.; Zheng, M.H.; Liu, Y.T.; Zhang, Y.S.; Zhu, X.B.; et al. Long-term ultrastable frequency dissemination via a 50-km spooled fiber link using a two-section DFB laser. *Chin. Opt. Lett.* **2024**, *22*, 013903. [CrossRef]
24. Williams, P.A.; Swann, W.C.; Newbury, N.R. High-stability transfer of an optical frequency over long fiber-optic links. *J. Opt. Soc. Am. B* **2008**, *25*, 1284–1293. [CrossRef]

25. Wang, B.; Zhu, X.; Gao, C.; Bai, Y.; Dong, J.W.; Wang, L.J. Square kilometre array telescope—Precision reference frequency synchronisation via 1f-2f dissemination. *Sci. Rep.* **2015**, *5*, 13851. [CrossRef] [PubMed]
26. Yin, Z.Q.; Zheng, M.H.; Zhang, C.B.; Guan, S.J.; Zhou, X.; Liu, Y.T.; Gang, Z.Y.; Nie, J.Q.; Zhang, Y.S.; Zhu, X.B.; et al. Stability-enhanced RF signal transmission over long fiber-optic links. *Chin. Opt. Lett.* **2024**, *22*, 053901. [CrossRef]

**Disclaimer/Publisher's Note:** The statements, opinions and data contained in all publications are solely those of the individual author(s) and contributor(s) and not of MDPI and/or the editor(s). MDPI and/or the editor(s) disclaim responsibility for any injury to people or property resulting from any ideas, methods, instructions or products referred to in the content.